On the use of finite fault solution for tsunami generation problems

Denys Dutykh, Dimitrios Mitsotakis, Xavier Gardeil

▶ **To cite this version:**

Denys Dutykh, Dimitrios Mitsotakis, Xavier Gardeil. On the use of finite fault solution for tsunami generation problems. 2010. hal-00509384v1

HAL Id: hal-00509384

https://hal.science/hal-00509384v1

Preprint submitted on 12 Aug 2010 (v1), last revised 12 Dec 2011 (v3)

HAL is a multi-disciplinary open access archive for the deposit and dissemination of scientific research documents, whether they are published or not. The documents may come from teaching and research institutions in France or abroad, or from public or private research centers.

L'archive ouverte pluridisciplinaire **HAL**, est destinée au dépôt et à la diffusion de documents scientifiques de niveau recherche, publiés ou non, émanant des établissements d'enseignement et de recherche français ou étrangers, des laboratoires publics ou privés.

ON THE USE OF FINITE FAULT SOLUTION FOR TSUNAMI GENERATION PROBLEMS

DENYS DUTYKH*, DIMITRIOS MITSOTAKIS, AND XAVIER GARDEIL

Abstract. The present study is devoted to the tsunami wave generation problem. The main goal of this work is two-fold. First of all, we propose a simple and computationally inexpensive model for the description of the sea bed displacement during an underwater earthquake, based on the finite fault solution for the slip distribution under some assumptions on the rupturing process dynamics. Once the bottom motion is reconstructed, we study waves induced on the free surface of the ocean. For this purpose we consider three different models approximating the Euler equations of the water wave theory. Namely, we deal with linearized Euler equations (also known as Cauchy-Poisson problem), a Boussinesq system and a weakly nonlinear model. An intercomparison of these approaches is performed. All developments in this study are illustrated on the real world example of the July 17, 2006 Java event.

1. Introduction

Tsunami waves have attracted a lot of attention by researchers. The scientific community's interest has especially increased since the Tsunami Boxing day [SB06] in December 2004, killing nearly 230,000 people in fourteen countries. This event has also incited countries concerned with tsunami hazard to develop respective Tsunami Warning Systems (TWS) [Syn05, Bas06]. Perhaps, the most elaborated warning system has been settled in the Pacific Ocean by efforts of NOAA's specialists [TGB+05, GBM+05]. Similarly, the Indian Ocean TWS has been developed by joint collaborative efforts of indonesian and german specialists.

An operational tsunami wave modeling tool is an indispensable part of any warning system [TGB+05, TDS07]. Henceforth, mathematical and numerical models in use should be improved to produce more accurate results in less CPU time [Ima96, TG97, DPD10]. In order to study the propagation of a tsunami wave usually an initial condition is needed to be provided to any numerical model designed for this purpose. The present study is an attempt to improve the initial tsunami waveform construction. The set of existing practices described in the literature constitutes the field of the so-called tsunami generation modeling [Ham73, TT01, DD07d, Dut07, DD09, DD10].

The Tsunami generation modelling was initiated in the early sixties by the prominent work of K. Kajiura [Kaj63], who proposed the use of the static sea bed displacement onto

Key words and phrases. water waves; tsunami waves; co-seismic displacements; moving bottom; tsunami generation.

* Corresponding author.

the free surface as an initial condition. Classically, the celebrated Okada [Oka85, Oka92] and sometimes Mansinha & Smylie[1] [MS67, MS71] solutions are used to compute the co-seismic sea bed displacements. This approach is still widely used by the tsunami wave modeling community. However, some progress has been recently made in this direction [OTM01, DD07d, Dut07, DD09, RLF+08, SF09, DPD10].

In the present study we propose to exploit some recent advances in the seismology to reconstruct better co-seismic displacements of a tsunamigenic earthquake. More precisely, we suggest the use of the so-called finite fault solution developed by C. Ji and his collaborators [BLM00, JWH02], based on static and seismic data inversion. This solution provides us with multiple fault segments of variable local slip, rake angle and several other parameters. By applying the Okada solution to each subfault, we reconstruct the sea bed displacement with higher resolution. To our knowledge, this technique was already employed to model Kuril islands tsunamis 15 November 2006 and 13 January 2007, cf. [RLF+08]. Since the Okada solution is constituted of relatively simple closed-form analytical expressions, all computations can be done efficiently enough to be used in a real-time TWS (cf. [WL08]). The obvious *sine qua non* condition is that the corresponding finite fault inversion is also performed in a reasonable time.

In our study we go further in reconstructing the dynamic sea bed displacement according to the rupture propagation speed and the rise time also provided by the finite fault solution. Constructed in this special way, sea bed displacements are then coupled with several water wave models. Among them, there is a novel weakly nonlinear solver based on a formulation involving the Dirichlet-to-Neumann operator which is computed approximately using the Fourier transform. The other two models considered here are the linearized free surface Euler equations and a Boussinesq type system. Developments presented in this paper are illustrated on the example of July 17, 2006 Java event [AKLV06]. However, we underline that the presented in this study methodology is quite general and can be applied to any other tsunamigenic earthquake for which a finite fault solution is available.

The paper is organized as follows. In Section 2 we describe the static and the dynamic sea bed displacements, while in Section 3 we present a simple approximate water wave solver with moving bottom. In Section 4 we study numerically the generation process of a real-world event. An intercomparison of the three models mentioned above is performed. A few important conclusions are drawn out in Section 5.

2. Co-seismic displacement construction

The problem of tsunami generation modeling is directly related to the problem of the bottom motion during an underwater earthquake. Traditionally, the so-called Okada solution [Oka85, Oka92] is used in cases of regimes characterized by an active fault of small or intermidiate size i.e. constituted by one or a few segments (e.g. the great Sumatra 2004 earthquake, [SB06, IAK+07]). In this case the resulting vertical displacement field is superposed at the free-surface. This approach is conventionally referred to as *passive tsunami generation* [DDK06], contrary to the *active generation* which explicitly involves the bottom

[1] In fact, Mansinha & Smylie solution is a particular case of the more general Okada solution.

Fault length, km	80.9
Fault width, km	40.0
Focal depth, km	20.0
Slip, m	2.5
Dip angle	10°
Slip angle	95°
Strike angle (CW from N)	289°

TABLE 1. Seismic fault parameters for the Java 2006 event. (The corresponding seismic moment can be taken $M_0 = 2.52 \times 10^{27} N \cdot m$ ($M_w = 7.56$).)

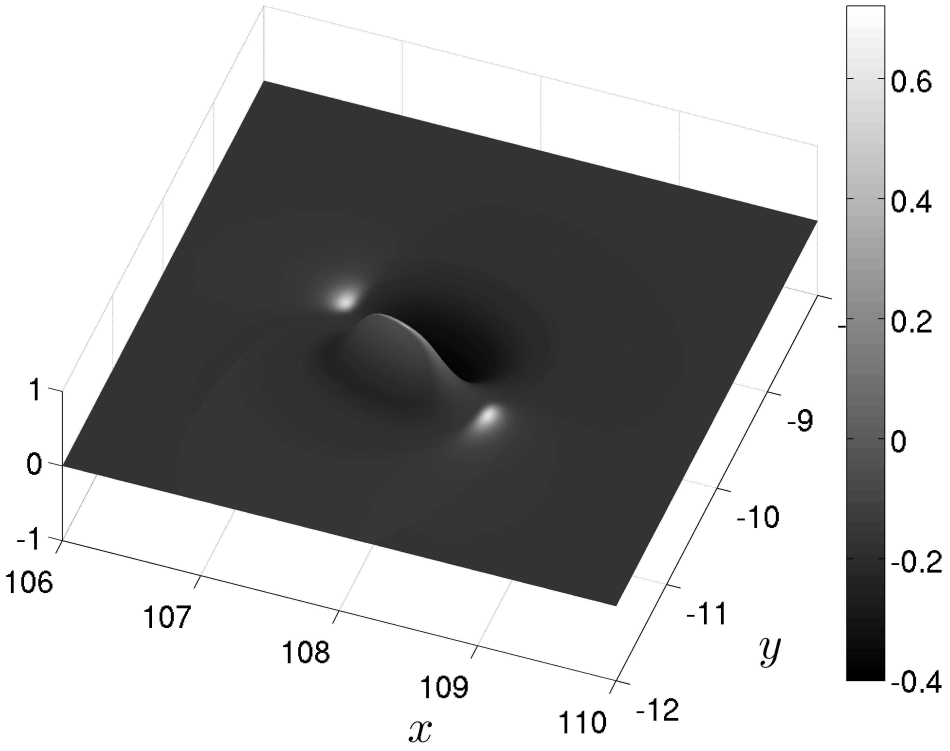

FIGURE 1. Static vertical displacement computed according to the single fault parameters of Table 1.

motion dynamics [DD07d]. Since in this study we decided to illustrate our methods on the example of July 17, 2006 Java event, we show on Figure 1 a typical single-fault based initial condition used for the corresponding tsunami wave modeling [Yal08]. The seismic parameters used to produce this vertical displacement are given in Table 1.

Remark 1. *The celebrated Okada solution [Oka85, Oka92] is based on two main ingredients — the dislocation theory of Volterra [Vol07] and Mindlin's fundamental solution for an elastic half-space [Min36]. Particular cases of this solution were known before Okada's work, for example the well-known Mansinha & Smylie's solution [MS67, MS71]. Usually all these particular cases differ by the choice of the dislocation and the Burger's vector orientation [Pre65]. We recall the basic assumptions behind this solution:*

- *Fault is immersed into the linear homogeneous and isotropic half-space*
- *Fault is a Volterra's type dislocation*
- *Dislocation has a rectangular shape*

For more information on Okada's solution we refer to [DD07d, DD07a, Dut07].

The finite fault solution is based on the multi-fault representation of the rupture [BLM00, JWH02]. The rupture complexity is reconstructed using a joint inversion of the static and seismic data. Fault's surface is parametrized by multiple segments with variable local slip, rake angle, rise time and rupture velocity. The inversion is performed in an appropriate wavelet transform space. The objective function is a weighted sum of L_1, L_2 norms and some correlative functions. With this approach seismologists are able to recover rupture slip details [BLM00, JWH02]. These available seismic information are exploited in this study to compute the sea bed displacements produced by an underwater earthquake with higher geophysical resolution.

The proposed approach will be directly illustrated on the Java's 2006 event. The July 17, 2006 Java's earthquake involved thrust faulting in the Java's trench and generated a tsunami wave that inundated the southern coast of Java [AKLV06, FKM+07]. The estimates of the size of the earthquake (cf. [AKLV06]) indicate a seismic moment of $6.7 \times 10^{20}\ N \cdot m$, which corresponds to the magnitude $M_w = 7.8$. Later this estimation was refined [Ji06] to $M_w = 7.7$. Like other events in this region, Java's event had an unusually low rupture speed of 1.0 – 1.5 km/s, and occurred near the up-dip edge of the subduction zone thrust fault. According to C. Ammon *et al* [AKLV06], most aftershocks involved normal faulting. The rupture propagated approximately 200 km along the trench with an overall duration of approximately 185 s. The fault's surface projection along with ocean ETOPO1 bathymetric map are shown in Figure 2. We note that Indian Ocean's bathymetry considered in this study varies between 7186 and 20 meters in the shallowest region.

Remark 2. *We have to mention that the finite fault inversion for this earthquake was also performed by the Caltech team [OK06]. They estimated the July 17, Southern Java earthquake magnitude was $M_w = 7.9$. In this study we do not present numerical simulations involving their data but it is straightforward to apply our algorithms to this case as well.*

2.1. **Static displacement.** In order to illustrate the advantages of the proposed approach we will compute also the static co-seismic displacements using the finite fault solution [Ji06]. The fault is considered to be the rectangle with vertices located at (109.20508° (Lon), −10.37387° (Lat), 6.24795 km (Depth)), (106.50434°, −9.45925°, 6.24795 km), (106.72382°, −8.82807°, 19.79951 km), (109.42455°, −9.74269°, 19.79951 km) (see Figure

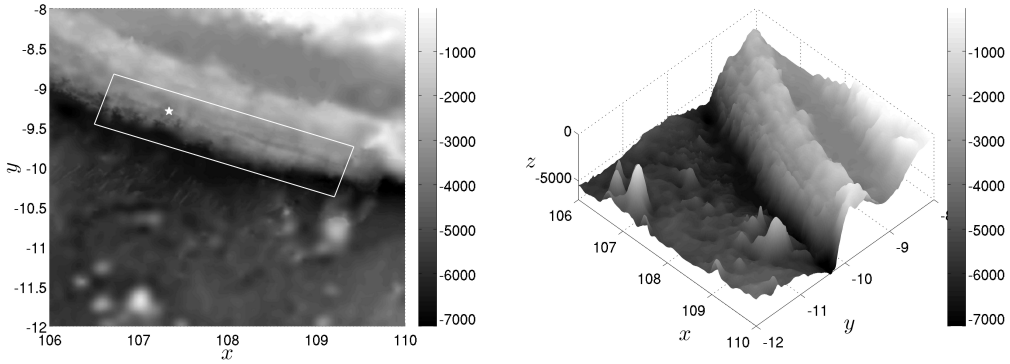

(a) Top view. (b) Bathymetry side view.

FIGURE 2. Surface projection of the fault's plane and the ETOPO1 bathymetric map of the region we study. The symbol $\star$ indicates the hypocenter's location at $(107.345°, -9.295°)$. The local Cartesian coordinate system is centered at the point $(108°, -10°)$. This region is located between $(106°, -8°)$ and $(110°, -12°)$.

P-wave celerity c_p, m/s	6000
S-wave celerity c_s, m/s	3400
Crust density ρ, kg/m^3	2700
Dip angle, δ	10.35°
Slip angle (CW from N)	288.94°

TABLE 2. Geophysical parameters used to model elastic properties of the subduction zone in the region of Java.

2 (a)). The fault's plane is conventionally divided into $N_x = 21$ subfaults along strike and $N_y = 7$ subfaults down the dip angle, leading to the total number of $N_x \times N_y = 147$ equal segments. Parameters such as subfault location (x_c, y_c), depth d_i, slip u and rake angle ϕ for each segment are given in Table 3 and can also be downloaded at [Ji06]. The common elastic constants to all subfaults parameters such as dip and slip angles are given in Table 2. (We note that the slip angle is measured traditionally in the counter-clockwise direction from the North. The relations between the elastic wave celerities c_p, c_s and Lamé coefficients λ, μ used in Okada's solution are outlined in Section 8.)

We compute the Okada's solution at the sea bottom (substituting $z = 0$ in the geophysical coordinate system) and taking the vertical component of the displacement field $\mathcal{O}_i(\vec{x}; \delta, \lambda, \mu, \ldots)$, where δ is the dip angle, λ, μ are the Lamé coefficients (see Appendix 8) and dots denote the dependence of the function $\mathcal{O}(\vec{x})$ on other 8 parameters, cf. [DD07d]. The resulting co-seismic vertical bottom displacement $\zeta(\vec{x})$ can be computed as a simple

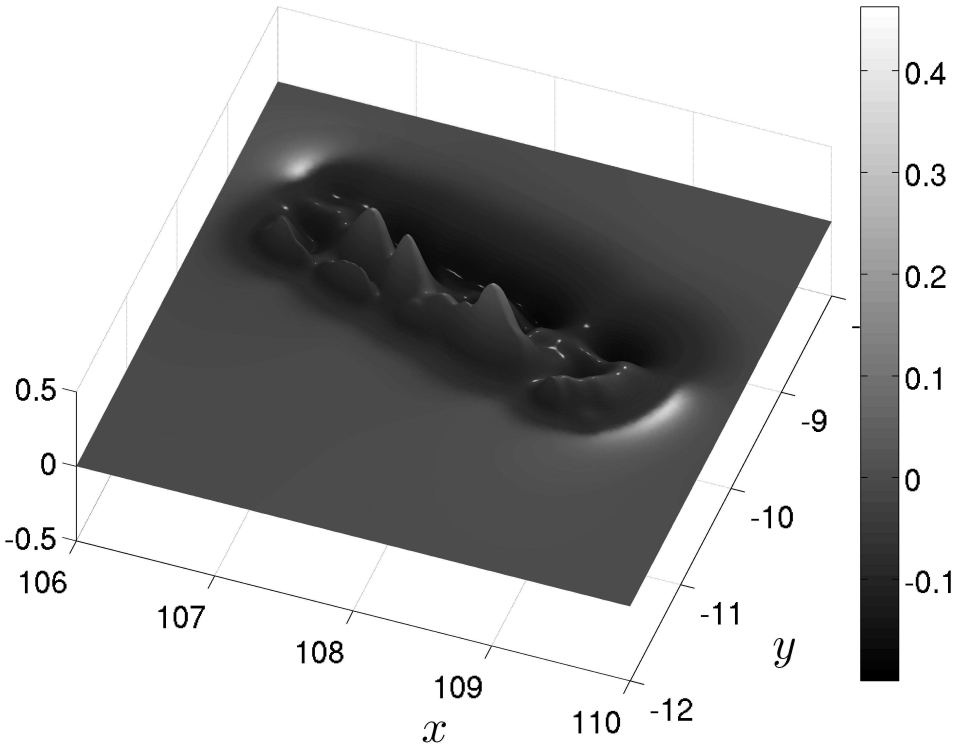

FIGURE 3. The vertical displacement of the finite fault solution, cf. [Ji06]. The corresponding seismic moment is $M_0 = 3.53 \times 10^{27}\ N \cdot m$ ($M_w = 7.65$).

superposition of subfault contributions:

$$\zeta(\vec{x}) = \sum_{i=1}^{N_x \times N_y} \mathcal{O}_i(\vec{x}; \delta, \lambda, \mu, \ldots)$$

The graph of $\zeta(\vec{x})$ is presented in Figure 3. The specific static displacement can be compared with the single fault classical approach depicted on Figure 1. It is worth to mention that more than one local extrema can be found in this solution due to a higher slip resolution.

Hereafter we will adopt the short-hand notation $\mathcal{O}_i(\vec{x})$ for the vertical displacement component of the Okada's solution for the i^{th} segment having in mind its dependence on various parameters from Tables 2 and 3.

2.2. **Dynamic co-seismic displacements.** Here, we go even further in the reconstruction of the bottom motion. By making some assumptions on the time dependence of displacement fields, we can have an insight into the dynamics of the sea bed motion.

The finite fault solution provides two additional parameters concerning the rupture dynamics of the July 17, 2006 event — the rupture velocity $v_r = 1.1\ km/s$ and the rise time

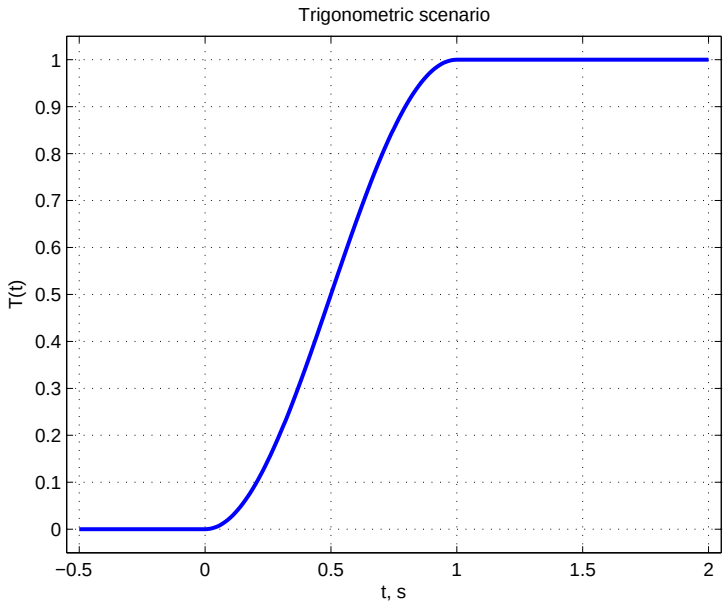

FIGURE 4. Trigonometric scenario with rise time $t_r = 1\ s$.

$t_r = 8\ s$. The epicenter is located at the point $\vec{x}_e = (107.345°, -9.295°)$ (cf. [Ji06]). Given the origin $\vec{x}_e$, the rupture velocity v_r and i^{th} subfault location $\vec{x}_i$ (the full list is provided in Table 3), we define the *subfault activation times* t_i needed for the rupture to achieve the corresponding segment i by the formulas:

$$t_i = \frac{||\vec{x}_e - \vec{x}_i||}{v_r}, \quad i = 1, \dots, N_x \times N_y.$$

We will also follow the pioneering idea of J. Hammack [Ham72, Ham73] developed later in [TT01, THT02, DD07d, DDK06, KDD07] where the maximum bottom deformation is achieved during some finite time (known as the rise time) according to a specific (in *ad hoc* manner) dynamic scenario. Various scenarios on the time dependence (instanteneous, linear, trigonometric, exponential, etc) can be found in [Ham73, DDK06, DD07d]. In this study we will adopt the trigonometric scenario which can be described by the formula:

$$T(t) = \mathcal{H}(t - t_r) + \frac{1}{2}\mathcal{H}(t)\mathcal{H}(t_r - t)\big(1 - \cos(\pi t/t_r)\big),$$

where $\mathcal{H}(t)$ is the Heaviside step function. For illustrative purposes this dynamic scenario is represented on Figure 4.

Finally, we put together all ingredients in order to construct the dynamic sea bed motion:

$$\zeta(\vec{x}, t) = \sum_{i=1}^{N_x \times N_y} \mathcal{H}(t - t_i) T(t - t_i) \mathcal{O}_i(\vec{x}). \tag{2.1}$$

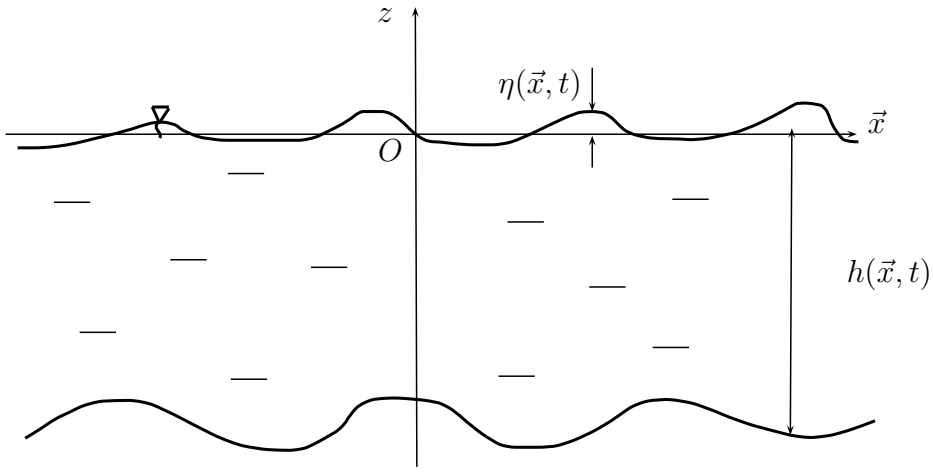

FIGURE 5. Sketch of the physical domain.

In the following sections we will present several approaches to couple this dynamic deformation with the hydrodynamic problem to predict waves induced on the ocean's free surface.

3. Fluid layer solution

Once the sea bed deformation is determined, a water wave problem has to be solved in order to compute the free surface motion induced by the ocean bottom shaking. Traditionally this difficulty is circumvented by the simple translation of the static bottom deformation onto the free surface [Kaj63], known as the passive generation approach [DDK06, KDD07]. In this section we present three approximate models to the water wave problem with moving bottom that we will use in combination with the finite-fault solution to study the tsunami generation problem.

3.1. Linearized Euler equations.

In the sequel we will consider an ideal incompressible fluid of constant density ρ in the domain $\Omega \subseteq \mathbb{R}^2$. The horizontal independent variables will be denoted by $\vec{x} = (x, y)$ and the vertical by z. The origin of the cartesian coordinate system is chosen such that the surface $z = 0$ corresponds to the still water level. The fluid is bounded below by the bottom $z = -h(\vec{x}, t)$ and above by the free surface $z = \eta(\vec{x}, t)$. Usually we assume that the total depth $H(\vec{x}, t) := h(\vec{x}, t) + \eta(\vec{x}, t)$ remains positive $H(\vec{x}, t) \geq h_0 > 0$ under the system dynamics $\forall t \in [0, T]$. The sketch of the physical domain is shown in Figure 5.

Remark 3. *Classically in water wave modeling, we make the assumption that the free surface is a graph $z = \eta(\vec{x}, t)$ of a single-valued function. It means in practice that we exclude some interesting phenomena, (e.g. wave breaking phenomena) which are out of the scope of this modeling paradigm.*

The linearized water wave problem consists of the following set of equations [Ham72, Ham73, DD07d]:

$$\Delta\phi = \nabla^2\phi + \partial_{zz}^2\phi = 0, \qquad (\vec{x}, z) \in \Omega \times [-h, 0], \tag{3.1}$$

$$\partial_t\eta - \partial_z\phi = 0, \qquad z = \eta(\vec{x}, t), \tag{3.2}$$

$$\partial_t\phi + g\eta = 0, \qquad z = \eta(\vec{x}, t), \tag{3.3}$$

$$\partial_t h + \partial_z\phi = 0, \qquad z = -h(\vec{x}, t). \tag{3.4}$$

This set of equations is also often referred in the literature as the Cauchy-Poisson (CP) problem after the pioneering work of A.-L. Cauchy [Cau27].

In view of the specific applications' requirements on analytical techniques, we will assume first that the domain $\Omega = \mathbb{R}^2$, i.e. unbounded in the horizontal extent, and the bottom has a special form:

$$h(\vec{x}, t) = h_0 - \zeta(\vec{x}, t),$$

where h_0 is some uniform depth and $\zeta(\vec{x}, t)$ is the sea bed displacement due to an underwater earthquake. In Section 2.2 one possible construction of the bottom displacement is proposed. Using integral transform methods (cf. [Ham73, TT01, DD07d, KDD07]), one can derive the following expression for the free surface elevation $\eta(\vec{x}, t)$:

$$\eta(\vec{x}, t) = \frac{\gamma^2}{2}\mathcal{F}^{-1}\Big\{\sum_{i=1}^{n} \frac{\mathcal{H}(t - t_i)\hat{\zeta}_i(\vec{k})}{(\gamma^2 - \omega^2)\cosh(|\vec{k}|h_0)}\big(\cos(\omega(t - t_i)) - \cos(\gamma(t - t_i)) + \mathcal{H}(t - t_i - t_0)[\cos(\omega(t - t_i - t_0)) + \cos(\gamma(t - t_i))]\big)\Big\},$$

where $\gamma = \dfrac{\pi}{t_r}$ and t_r is the rise time defined in Section 2.2. A similar expression can be also derived for the velocity potential $\phi(\vec{x}, z, t)$, however we do not directly need it in our study.

This semi-analytical solution will be used below in numerical simulations. It has a big advantage of being simple and, thus, computationally inexpensive. However, the flat bottom assumption ($h(\vec{x}) = h_0 = const$) prevents us from using this solution beyond some small evolution times. The validity of this approximation has already been addressed in the literature [KDD07, SF09] and will be discussed at some point below.

3.2. **The weakly-nonlinear model.** A tsunami wave during its generation is well described even by the CP problem [DD07d, KDD07, SF09]. The main reason for this simplicity is the fact that a wave of a half meter amplitude represents only a tiny perturbation of a 4000 m water column. However, the real life bathymetry is generally complex and may contain simultaneously various scales. For example, the subduction zone bathymetry represented on Figure 2 ranges from 7000 to 20 m and thus, nonlinear effects may be locally important. In order to take into account all realistic bathymetric features and study at least the initial stages of a tsunami propagation we propose below a new numerical model.

Here we consider the physical setting and notation from Section 3.1. The governing equations of the classical water wave problem are the following [Lam32, Sto58, Mei94,

Whi99]:

$$\Delta\phi = \nabla^2\phi + \partial_{zz}^2\phi = 0, \qquad (\vec{x}, z) \in \Omega \times [-h, \eta], \tag{3.5}$$

$$\partial_t\eta + \nabla\phi \cdot \nabla\eta - \partial_z\phi = 0, \qquad z = \eta(\vec{x}, t), \tag{3.6}$$

$$\partial_t\phi + \tfrac{1}{2}|\nabla\phi|^2 + \tfrac{1}{2}(\partial_z\phi)^2 + g\eta = 0, \qquad z = \eta(\vec{x}, t), \tag{3.7}$$

$$\partial_t h + \nabla\phi \cdot \nabla h + \partial_z\phi = 0, \qquad z = -h(\vec{x}, t), \tag{3.8}$$

with ϕ the velocity potential, g the acceleration due to gravity force and $\nabla = (\partial_x, \partial_y)$ denotes the gradient operator in horizontal Cartesian coordinates.

Fluid incompressibility and flow irrotationality assumptions lead to the Laplace equation (3.5) for the velocity potential $\phi(\vec{x}, z, t)$. The main difficulty of the water wave problem lies on the boundary conditions. Equations (3.6) and (3.8) express the free surface and bottom impermeability, while the Bernoulli condition (3.7) expresses the free surface isobarity respectively.

Function $h(\vec{x}, t)$ represents the ocean's bathymetry (depth below the still water level, see Figure 5) and is assumed to be known. The dependence on time is included in order to take into account the bottom motion during an underwater earthquake [DD07a, DD07d, DDK06, Dut07]. In this study the bathymetry is decomposed into the static part $h_0(\vec{x})$ (given e.g. by the ETOPO1 database, cf. Figure 2) and of the dynamic sea bed displacement $\zeta(\vec{x}, t)$ constructed above (2.1):

$$h(\vec{x}, t) = h_0(\vec{x}) - \zeta(\vec{x}, t). \tag{3.9}$$

Remark 4. *Surface tension effects can also be included in the water wave problem. In this case, the Bernoulli condition (3.7) has to be modified:*

$$\partial_t\phi + \tfrac{1}{2}|\nabla\phi|^2 + \tfrac{1}{2}(\partial_z\phi)^2 + g\eta = \frac{\sigma}{\rho}\nabla \cdot \left(\frac{\nabla\eta}{\sqrt{1 + |\nabla\eta|^2}}\right), \qquad z = \eta(\vec{x}, t),$$

where σ is the surface tension coefficient. However, this effect is negligible for the applications considered in the present study and will be ignored.

Remark 5. *Recently, some weak dissipative effects have also beed included into the classical water wave problem (3.5) – (3.8). For more details on the visco-potential formulation we refer to [DDZ08, DD07c, Dut07, Dut09b, Dut09a].*

For the exposition below we will need also to compute unitary exterior normals to the fluid domain. It is straightforward to obtain the following expressions for the normals at the free surface and bottom respectively:

$$\hat{n}_f = \frac{1}{\sqrt{1 + |\nabla\eta|^2}} \begin{vmatrix} -\nabla\eta \\ 1 \end{vmatrix}, \qquad \hat{n}_b = \frac{1}{\sqrt{1 + |\nabla h|^2}} \begin{vmatrix} -\nabla h \\ -1 \end{vmatrix}.$$

In 1968 V. Zakharov proposed a different formulation of the water wave problem based on the trace of the velocity potential at the free surface [Zak68]:

$$\varphi(\vec{x}, t) := \phi(\vec{x}, \eta(\vec{x}, t), t).$$

This variable plays a role of the generalized momentum in the Hamiltonian description of water waves [Zak68, DB06]. The second canonical variable is the free surface elevation η.

Another important ingredient is the normal velocity at the free surface v_n which is defined as:

$$v_n(\vec{x},t) := \sqrt{1+|\nabla\eta|^2}\,\frac{\partial\phi}{\partial\hat{n}_f}\bigg|_{z=\eta} = (\partial_z\phi - \nabla\phi\cdot\nabla\eta)|_{z=\eta}\,. \tag{3.10}$$

Dynamic boundary conditions (3.6) and (3.7) at the free surface can be rewritten in terms of φ, v_n and η [CSS92, CS93, FCKG05]:

$$\begin{aligned} \partial_t\eta - \mathcal{D}_\eta(\varphi) &= 0,\\ \partial_t\varphi + \tfrac{1}{2}|\nabla\varphi|^2 + g\eta - \tfrac{1}{2(1+|\nabla\eta|^2)}\big[\mathcal{D}_\eta(\varphi)+\nabla\varphi\cdot\nabla\eta\big]^2 &= 0. \end{aligned} \tag{3.11}$$

Here we introduced the so-called Dirichlet-to-Neumann operator (D2N) [CM85, CS93] which maps the velocity potential at the free surface φ to the normal velocity v_n:

$$\mathcal{D}_\eta: \qquad \varphi \mapsto v_n = \sqrt{1+|\nabla\eta|^2}\,\tfrac{\partial\phi}{\partial\hat{n}_f}\Big|_{z=\eta}$$

$$\left|\begin{aligned} \nabla^2\phi + \partial_{zz}^2\phi &= 0, \quad (\vec{x},z)\in\Omega\times[-h,\eta],\\ \phi &= \varphi, \quad z=\eta,\\ \sqrt{1+|\nabla h|^2}\frac{\partial\phi}{\partial\hat{n}_b} &= \partial_t h, \quad z=-h. \end{aligned}\right.$$

The name of this operator comes from the fact that it makes a correspondance between Dirichlet data φ and Neumann data $\sqrt{1+|\nabla\eta|^2}\,\frac{\partial\phi}{\partial\hat{n}_f}\Big|_{z=\eta}$ at the free surface. For the sake of completeness we provide in Section 7 the complete derivation of the Zakharov's formulation formulation for the water wave problem.

3.2.1. *Numerical estimation of D2N operator.* It was shown that the water wave problem can be reduced to a system of two PDEs governing the evolution of the canonical variables η and φ. In order to solve this system of equations we have to be able to compute efficiently the quantity $\mathcal{D}_\eta(\varphi)$. In this section we present a simple approximate method for the computation of the Dirichlet-to-Neumann (D2N) operator appropriate for tsunami generation problems extending the linearized Euler model. This approach is based on the extensive use of the Fourier transform. On the discrete level this transformation can be efficiently implemented thanks to the Fast Fourier Transform (FFT) algorithm [CT65, FJ05].

The direct $\mathcal{F}$ and inverse $\mathcal{F}^{-1}$ Fourier transforms in 2D are defined as follows:

$$\mathcal{F}[f] = \hat{f}(\vec{k}) = \int_{\mathbb{R}^2} f(\vec{x})e^{-i\vec{k}\cdot\vec{x}}\,d\vec{x}, \quad \mathcal{F}^{-1}[\hat{f}] = f(\vec{x}) = \frac{1}{(2\pi)^2}\int_{\mathbb{R}^2}\hat{f}(\vec{k})e^{i\vec{k}\cdot\vec{x}}\,d\vec{k}.$$

In this study, the Fourier transform of a function f will be denoted $\hat{f} = \mathcal{F}[f]$.

Let us recall the problem we have to solve:

$$\nabla^2\phi + \partial_{zz}^2\phi = 0, \quad (\vec{x}, z) \in \Omega \times [-h, \eta], \tag{3.12}$$

$$\phi = \varphi, \quad z = \eta, \tag{3.13}$$

$$\sqrt{1 + |\nabla h|^2}\frac{\partial\phi}{\partial\hat{n}_b} = \partial_t h, \quad z = -h. \tag{3.14}$$

Once the function ϕ is determined, we have to compute its normal derivative at the free surface $\sqrt{1 + |\nabla\eta|^2}\left.\dfrac{\partial\phi}{\partial\hat{n}_f}\right|_{z=\eta}$.

Since a tsunami wave induces a special flow regime in which the horizontal extent is much more important than variations in vertical direction, we can apply the Fourier transform to the Laplace equation (3.12) as if it were posed in a strip-like domain:

$$\frac{d^2\hat{\phi}}{dz^2} - |\vec{k}|^2\hat{\phi} = 0.$$

The general exact solution to this ODE can be easily computed:

$$\hat{\phi}(\vec{k}; z) = A(\vec{k})\cosh(|\vec{k}|z) + B(\vec{k})\sinh(|\vec{k}|z). \tag{3.15}$$

Two unknown functions $A(\vec{k})$ and $B(\vec{k})$ have to be determined from boundary conditions (3.13), (3.14). For our convenience we will rewrite the Neumann boundary condition at the bottom (3.14) in this form:

$$\left.\frac{\partial\phi}{\partial z}\right|_{z=-h} = -\partial_t h - \nabla\phi|_{z=-h} \cdot \nabla h \equiv f(\vec{x}, t). \tag{3.16}$$

The right-hand side will be denoted by $f(\vec{x}, t)$ that implicitly depends on the solution ϕ.

The application of the boundary conditions leads to the following system of linear equations:

$$\begin{aligned} \cosh(|\vec{k}|\eta)A(\vec{k}) + \sinh(|\vec{k}|\eta)B(\vec{k}) &= \hat{\varphi} \\ -|\vec{k}|\sinh(|\vec{k}|h)A(\vec{k}) + |\vec{k}|\cosh(|\vec{k}|h)B(\vec{k}) &= \hat{f}, \end{aligned}$$

which can be easily solved:

$$A(\vec{k}) = \frac{\hat{\varphi}\cosh(|\vec{k}|h) - \hat{f}\dfrac{\sinh(|\vec{k}|\eta)}{|\vec{k}|}}{\cosh(|\vec{k}|H)}, \quad B(\vec{k}) = \frac{\hat{\varphi}\sinh(|\vec{k}|h) + \hat{f}\dfrac{\cosh(|\vec{k}|\eta)}{|\vec{k}|}}{\cosh(|\vec{k}|H)},$$

where $H = h + \eta$ is the total water depth. The knowledge of these functions leads the determination of the velocity potential in the whole domain thanks to general solution (3.15).

Finally, we compute the normal velocity at the free surface $\mathcal{D}_\eta(\varphi) = \partial_z\phi|_{z=\eta} - \nabla\phi|_{z=\eta} \cdot \nabla\eta$. If we compute this quantity in Fourier transform space, the answer will be given

immediately by the inverse transformation $\mathcal{F}^{-1}$. The first term is readily given by the formula:

$$\partial_z \hat{\phi}\Big|_{z=\eta} = \hat{\varphi}|\vec{k}| \tanh(|\vec{k}|H) + \hat{f}\,\mathrm{sech}(|\vec{k}|H).$$

To compute the second term we use the following approximate expression:

$$\widehat{\nabla\phi|_{z=\eta}\cdot\nabla\eta} = \mathcal{F}\Big[\mathcal{F}^{-1}\big[i\vec{k}\hat{\varphi}\big]\cdot\mathcal{F}^{-1}\big[i\vec{k}\hat{\eta}\big]\Big]. \tag{3.17}$$

Remark 6. *From equation (3.16) follows that the function $f(\vec{x},t_n)$ depends implicitly on the unknown solution $\phi(\vec{x},z,t_n)$. In order to resolve this apparent contradiction, we apply a fixed point-type iteration initialized with the value of $f(\vec{x},t_{n-1})$ from the previous time step:*

$$\hat{f}^{k+1} = -\widehat{\partial_t h} - \mathcal{F}\Big[\nabla\phi|_{z=-h}(\hat{f}^k)\cdot\nabla h\Big], \quad \hat{f}^0 = \hat{f}(\vec{k};t_{n-1}).$$

The last product is computed in the physical space:

$$\mathcal{F}\Big\{\nabla\phi|_{z=-h}(f^k)\cdot\nabla h\Big\} = \mathcal{F}\Big[\mathcal{F}^{-1}\big[\widehat{\nabla\phi}\Big|_{z=-h}(\hat{f}^k)\big]\cdot\nabla h\Big],$$

where after simple computations one obtains:

$$\widehat{\nabla\phi}\Big|_{z=-h}(f^k) = i\vec{k}\Big[\hat{\varphi}\,\mathrm{sech}(|\vec{k}|H) - \hat{f}^k\frac{\tanh(|\vec{k}|H)}{|\vec{k}|}\Big].$$

Our numerical experiments show that this iterative procedure is convergent and the tolerance $\varepsilon := ||f^{k+1}-f^k||_\infty \le 10^{-5}$ is reached after four iterations in average.

The resulting model is only weakly nonlinear since some information about the solution is lost when we solve the Laplace equation (3.12) in a strip-like domain. However, the WN model contrary to the CP model not only takes into account some nonlinear effects but can be also efficiently applied to cases with realistic bathymetry. We note that this model is analogous at some point to the first order approximation model proposed in [GN07].

3.3. **Time integration.** The application of the previously derived Fourier type spectral method to equations (3.11) governing the evolution of canonical variables η and φ, leads to a system of ordinary differential equations, i.e.

$$\Phi_t = \mathcal{A}(t,\Phi), \qquad \Phi(t_0) = \Phi_0. \tag{3.18}$$

In order to integrate numerically this system of ODEs we apply an integrating multiplier method analogous to one used in [FCKG05, XG09]. This method appears to decrease the ODEs system stiffness and, therefore, allows for efficient application of explicit time integration schemes. We start by extracting the linear part of equations (3.18):

$$\Phi_t + \mathcal{L}\cdot\Phi = \mathcal{N}(\Phi), \tag{3.19}$$

where $\mathcal{L} = \begin{pmatrix} 0 & -\frac{\omega^2}{g} \\ g & 0 \end{pmatrix}$ and $\omega = \sqrt{g|\vec{k}|\tanh(|\vec{k}|h_0)}$ is the wave frequency corresponding to the wave number $|\vec{k}|$. For a general bathymetry we choose the constant h_0 to be the mean

water depth. The term $\mathcal{N}(\Phi)$ incorporates remaining nonlinear terms:

$$\mathcal{N}(\Phi) = \begin{pmatrix} \mathcal{F}\big\{\mathcal{D}_\eta(\varphi)\big\} - \frac{\omega^2}{g}\hat{\varphi} \\ \mathcal{F}\Big\{\frac{1}{2(1+|\nabla\eta|^2)}\big[\mathcal{D}_\eta(\varphi) + \nabla\varphi\cdot\nabla\eta\big]^2 - \frac{1}{2}|\nabla\varphi|^2\Big\} \end{pmatrix}.$$

Linear terms can be integrated exactly by the following change of variables:

$$\Psi(t) := e^{\mathcal{L}(t-t_0)}\Phi(t), \qquad e^{\mathcal{L}(t-t_0)} = \begin{pmatrix} \cos(\omega(t-t_0)) & -\frac{\omega}{g}\sin(\omega(t-t_0)) \\ \frac{g}{\omega}\sin(\omega(t-t_0)) & \cos(\omega(t-t_0)) \end{pmatrix}.$$

Consequently, we solve in practice the following system of ODEs:

$$\Psi_t = e^{\mathcal{L}(t-t_0)}\mathcal{N}\big(e^{-\mathcal{L}(t-t_0)}\Psi\big) \equiv \mathcal{B}(t,\Psi), \qquad \Psi(t_0) = \Phi_0.$$

This simple modification allows us to take larger CFL number, thus, improving the overall time stepping performance.

Finally, the last system of ODEs is discretized with the standard fourth-order Runge-Kutta (RK4) scheme [HNW09]:

$$\begin{aligned} \Psi_{n+1} &= \Psi_n + \tfrac{1}{6}h(k_1 + 2k_2 + 2k_3 + k_4), \\ k_1 &= \mathcal{B}(t_n, \Psi_n), \\ k_2 &= \mathcal{B}(t_n + \tfrac{1}{2}h, \Psi_n + \tfrac{1}{2}hk_1), \\ k_3 &= \mathcal{B}(t_n + \tfrac{1}{2}h, \Psi_n + \tfrac{1}{2}hk_2), \\ k_4 &= \mathcal{B}(t_n + h, \Psi_n + hk_3), \end{aligned} \tag{3.20}$$

where the subscript refers to the discrete time instance $\Psi_n := \Psi(t_n)$ and h is the discrete time step: $t_{n+1} = t_n + h$.

We have to mention that in the computations we will present below, we use a Runge-Kutta (4,5) scheme with an adaptive time step control (cf. [DP80]). However, fundamentally it is not so different from the classical RK4 scheme (3.20) described above.

3.4. **The BBM-BBM type system.** When the so-called long wave approximation is applied to the water wave problem (3.5) – (3.8), one obtains the well-known nonlinear shallow water (or Saint-Venant) equations [dSV71, Sto58, Whi99] which have been extensively used for tsunami simulations [Ima96, TG97, TS98, DKK07, DPD10]. If we go further in asymptotic expansions, some dispersive effects can be included and generally the resulting system is referred to as Boussinesq equations [Bou72, MBS03, DD07b, DMS07, DMS09].

In this study we will also use a Boussinesq system of BBM-BBM type with variable bottom derived in [Mit09]. The system in dimensional variables can be written as:

$$\begin{aligned} \eta_t + \nabla\cdot((h_0+\eta)\vec{u}) + \nabla\cdot\{Ah_0^2[\nabla(\nabla h_0\cdot\vec{u}) + \nabla h_0\nabla\cdot\vec{u}] - bh_0^2\nabla\eta_t\} + \\ A\nabla\cdot(h_0^2\nabla\zeta_t) + \zeta_t &= 0, \\ \vec{u}_t + g\nabla\eta + \tfrac{1}{2}\nabla|\vec{u}|^2 + Bgh_0[\nabla(\nabla h\cdot\nabla\eta) + \nabla h_0\Delta\eta] - dh_0^2\Delta\vec{u}_t \\ -Bh_0\nabla\zeta_{tt} &= 0, \end{aligned} \tag{3.21}$$

where A, B, b and d are constants defined as:

$$A = \sqrt{\frac{2}{3}} - \frac{2}{3}, \quad B = 1 - \sqrt{\frac{2}{3}}, \quad b = d = \frac{1}{6}.$$

The variable $\vec{u}(\vec{x},t)$ denotes the horizontal velocity of the fluid at $z=-h+\sqrt{2/3}(\eta+h)$, and bathymetry variables $h(\vec{x},t)$, $h_0(\vec{x})$, $\zeta(\vec{x},t)$ defined in Senction 2.

We integrate numerically system (3.21) using the standard Galerkin/finite element method with $\mathbb{P}1$ elements for the spatial discretization coupled with the 2nd order explicit Runge-Kutta method for the temporal discretization [HNW09].

In order to obtain a well-posed problem, we impose homogeneous Dirichlet boundary conditions which absorb partially the wave while reflecting only small amplitude oscillatory waves. Moreover, the specific numerical method appears to converge with optimal rate in the L^2 and L^∞ norms whether we consider structured or unstructured grids contrary to the respective initial boundary values problems with zero Dirichlet boundary conditions on $\vec{u}$ for Peregrine's system [Per67] where the analogous numerical method converges with suboptimal orders on structured and unstructured grids. For more information on the properties and the implementation of the numerical method for the BBM-BBM type system we refer to [DMS07, Mit09].

4. Numerical results

In this section we compare the propagation of a solitary wave when it is used as an initial condition in both CP and WN models. Moreover, we study the generation and the initial stages of the propagation of the tsunami wave of July 17, 2006 event. We also present a comparison between the WN, CP and Boussinesq models.

4.1. **Solitary wave propagation.**

Before performing the Java 2006 tsunami generation simulations, we study the propagation of a solitary wave solution to the full water wave problem using WN and CP models. The initial condition is provided by the well-known Tanaka's method [Tan86].

Consider the two-dimensional water wave problem in a channel of uniform depth $h_0 = const$. Since we look for travelling wave solutions, the flow field can be reduced to the steady state by choosing a frame of reference moving with the wave speed c.

After passing to dimensionless variables, there remains only one scaling parameter — the Froude number which is traditionally defined as $\mathrm{Fr} := \dfrac{c}{\sqrt{gh_0}}$. Hereafter, governing equations are considered in dimensionless form.

The complex velocity potential is classically introduced as $w=\phi+i\psi$, where ψ is the stream function. We choose $\phi=0$ at the crest and $\psi=0$ at the bottom. The fluid region is then mapped onto the strip $0<\psi<1$, $-\infty<\phi<\infty$ on the plane w with $\psi=1$ corresponding to the free surface.

We introduce the quantity $\Omega=\log\dfrac{dw}{dz}=\tau-i\theta$, where θ is the angle between the velocity vector and horizontal axis Ox. The real part τ is expressed in terms of the velocity magnitude q as $\tau=\log q$.

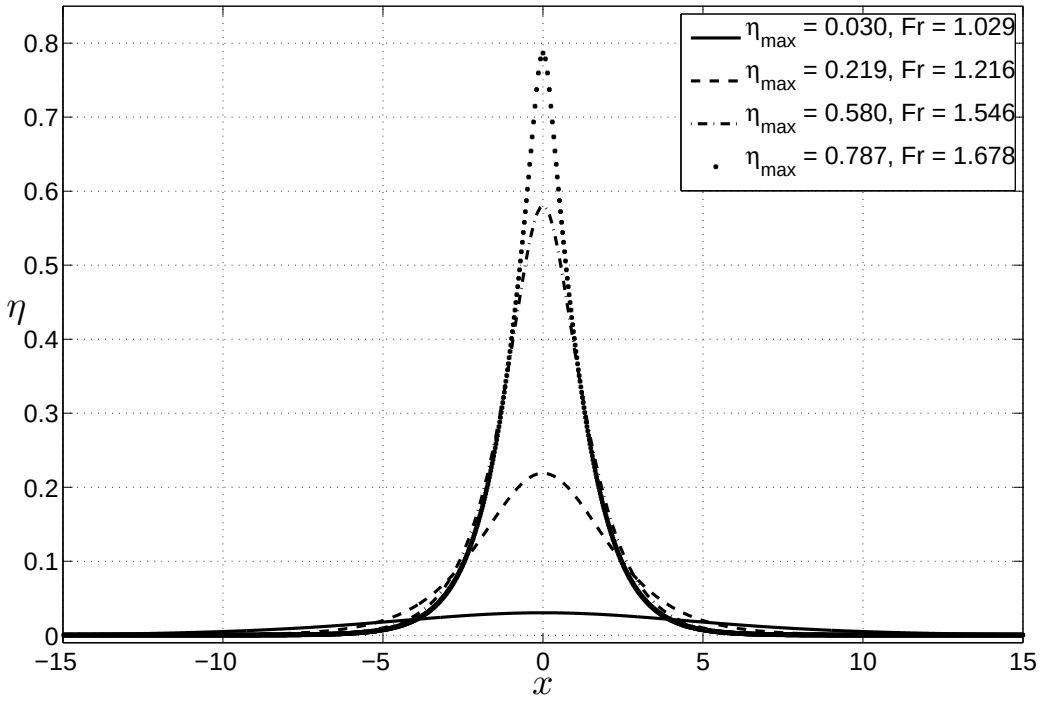

FIGURE 6. Solitary wave solutions of various amplitudes for the full water wave problem.

Boundary conditions to be satisfied are the Bernoulli condition at the free surface and the bottom impermeability which are expressed as

$$\frac{dq^3}{d\phi} = -\frac{3}{\mathrm{Fr}^2}\sin\theta, \quad \text{on } \psi = 1 \qquad \text{and} \qquad \theta = 0, \quad \text{on } \psi = 0. \tag{4.1}$$

Consequently, the problem now is transformed to the determination of complex function Ω, analytic with respect to w within the region of the unit strip $0 < \psi < 1$, decays at infinity and satisfies two boundary conditions (4.1). By applying Cauchy's integral theorem, one can find the following integral equation on the free surface $\psi = 1$:

$$-\theta(\phi) - \frac{2}{\pi}\int_{-\infty}^{\infty} \frac{\theta(\phi)}{(\varphi-\phi)^2+4}\,d\varphi = -\frac{1}{\pi}\int_{-\infty}^{\infty} \frac{(\varphi-\phi)\tau(\varphi)}{(\varphi-\phi)^2+4}\,d\varphi + \frac{1}{\pi}\mathrm{p.v.}\int_{-\infty}^{\infty} \frac{\tau(\varphi)}{\varphi-\phi}\,d\varphi,$$

where $\tau(\phi)$ and $\theta(\phi)$ denote the traces of corresponding functions at the free surface $\psi = 1$.

The last integral equation is solved iteratively with a method analogous to the one proposed [Tan86]. The convergence is tested with respect to the Froude number. Several solitary wave solutions computed in this way are plotted on Figure 6 for illustrative purposes.

In order to illustrate the advantages of the proposed weakly-nonlinear model over the classical CP solution, we let a solitary wave with amplitude $A/h_0 = 0.1$ propagate up to $T = 80$.

We recall that the classical CP solution of (3.1)–(3.4) corresponding to the initial free surface height $\eta|_{t=0} = \eta_0(x)$ and the velocity potential distribution at the free surface $\varphi|_{t=0} = \varphi_0(x)$, takes the following form:

$$\eta(\vec{x},t) = \mathcal{F}^{-1}\Big\{\hat{\eta}_0(\vec{k})\cos(\omega t) + \frac{\omega}{g}\hat{\varphi}_0(\vec{k})\sin(\omega t)\Big\},$$

$$\phi(\vec{x},z,t) = \mathcal{F}^{-1}\Big\{\big(\hat{\varphi}_0(\vec{k})\cos(\omega t) - \frac{g}{\omega}\hat{\eta}_0(\vec{k})\sin(\omega t)\big) \big(\cosh(|\vec{k}|z) + \tanh(|\vec{k}|h)\sinh(|\vec{k}|z)\big)\Big\},$$

where $\hat{\eta}_0(\vec{k}) = \mathcal{F}\{\eta_0(\vec{x})\}$ and $\hat{\varphi}_0(\vec{k}) = \mathcal{F}\{\varphi_0(\vec{x})\}$ are Fourier transforms of initial conditions.

The solution profiles of both models are presented in Figures 7 (a)–(e). One can observe that the weakly-nonlinear method retains much better the solitary wave while shedding a small dispersive tail behind. The CP solution gradually transforms the initial wave into the dispersive tail according to the linear nature of equations (3.1)–(3.4). In Figure 7 (f) we present the normalized amplitude error defined as:

$$\epsilon(t) := \frac{|\max_x\{\eta(x,t)\} - A/h_0|}{A/h_0},$$

where $\max_x\{\eta(x,t)\}$ denotes the discrete maximum of the numerical solution and $A/h_0 = 0.1$ is the exact solitary wave amplitude. In both computations a uniform grid of 512 nodes is used. Here again we notice a better performance of the WN solver compared to that of the CP solution. This specific experiment shows that the WN model includes necessary nonlinear effects for the study of tsunami generation and propagation phenomena.

4.2. **The July 17, 2006 tsunami generation simulation.** The main purpose of this study is to present a novel methodology of tsunami generation. This approach is illustrated on the example of 17 July 2006 Java tsunami since this event is not completely understood yet and there is an available finite fault solution for the respective underwater earthquake.

In this section we show some numerical results on water waves generated by moving bottom. Namely, we exploit the bottom motion (2.1) constructed in Section 2.2. The corresponding hydrodynamic problem is solved by the three methods discussed above: the linearized water wave problem (CP), BBM-BBM system and the new WN model.

The solution given by the WN model and the exact solutions to the linearized Euler equations (3.1) – (3.4) are computed on a uniform grid of 512×512 points. The time step Δt is chosen adaptively according to the RK(4,5) method proposed in [DP80]. The BBM-BBM system is solved on a triangular unstructured grid of 86276 elements. For the time integration the classical RK2 scheme [HNW09] with the time step $\Delta t = 0.5\ s$ is employed.

Several snapshots of the free surface elevation computed by the WN model are shown in Figures 8 (a) – (f). Analogous contour plots of the solutions of the CP and the BBM-BBM models are almost identical and differences cannot be observed within the graphical accuracy and therefore are not presented here. The parameters of the bottom motion, bathymetry and computational domain geometry were explained in Section 2.

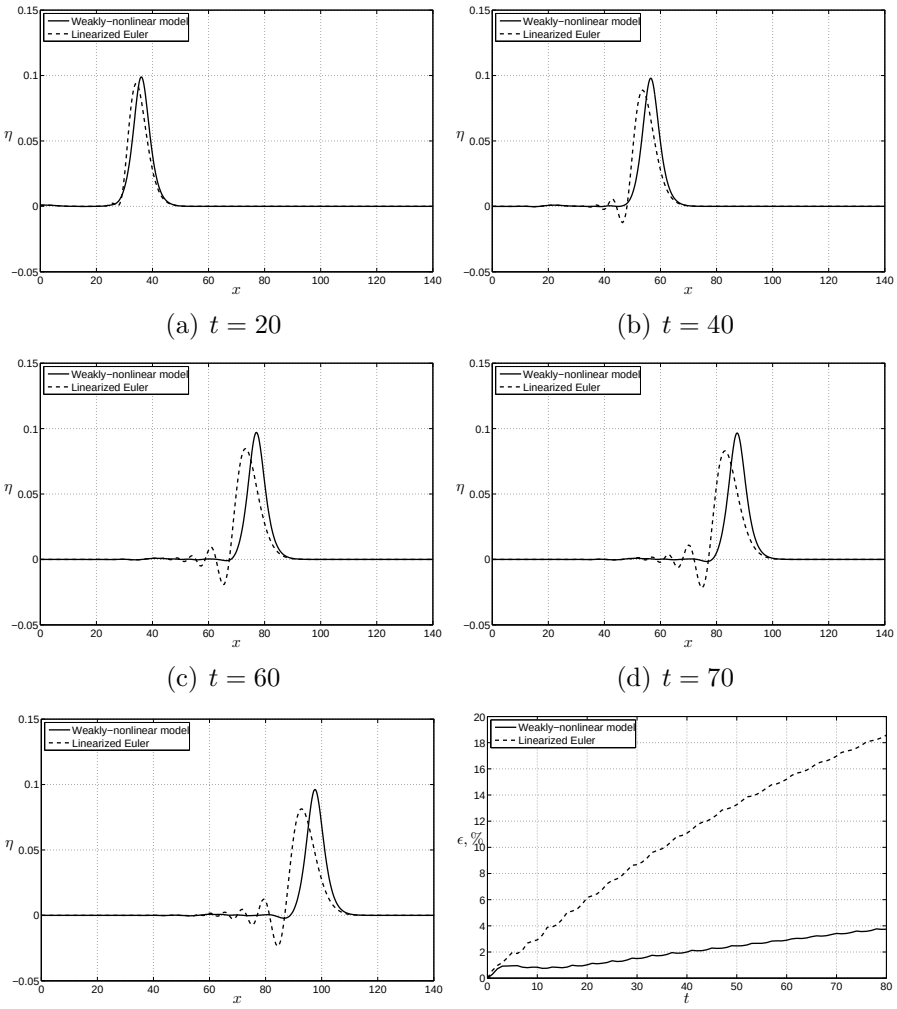

(a) $t = 20$ (b) $t = 40$

(c) $t = 60$ (d) $t = 70$

(e) $t = 80$ (f) Amplitude error

FIGURE 7. Tanaka's solution propagation with the weakly-nonlinear method (solid line) and Cauchy-Poisson (CP) solution (dashed line). Solitary wave amplitude is $A/h_0 = 0.1$.

In this computation, we see a complex process of simultaneous wave evolution together with rupture propagation during approximately 210 s. Namely, the free surface deformed by first subfaults starts to evolve while the rupture propagates along the fault. This kind of fluid/moving bottom interaction cannot be described in the passive generation framework.

In order to perform the intercomparison among the three models described above we put six numerical wave gauges at the following locations: (a) (107.2°, −9.388°), (b) (107.4°, −9.205°), (c) (107.6°, −9.648°), (d) (107.7°, −9.411°), (e) (108.3°, −10.02°), (f) (108.2°, −9.75°). The locations of the wave gauges is represented by the symbol ⋄ on Figure 9

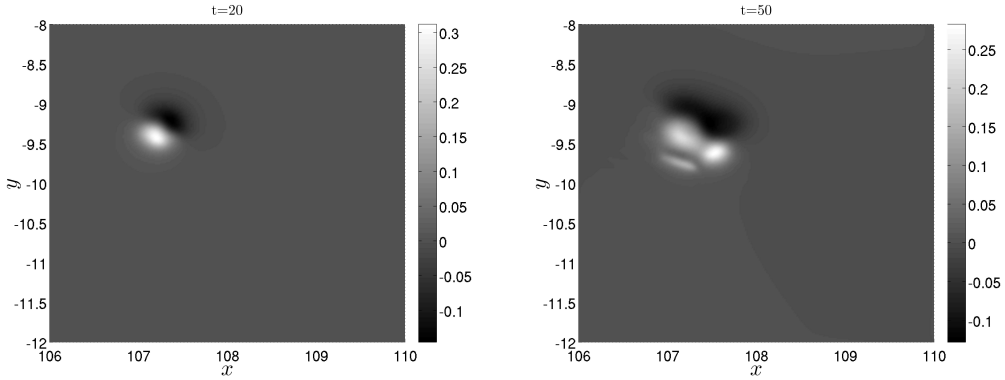

(a) $t = 20\ s$

(b) $t = 50\ s$

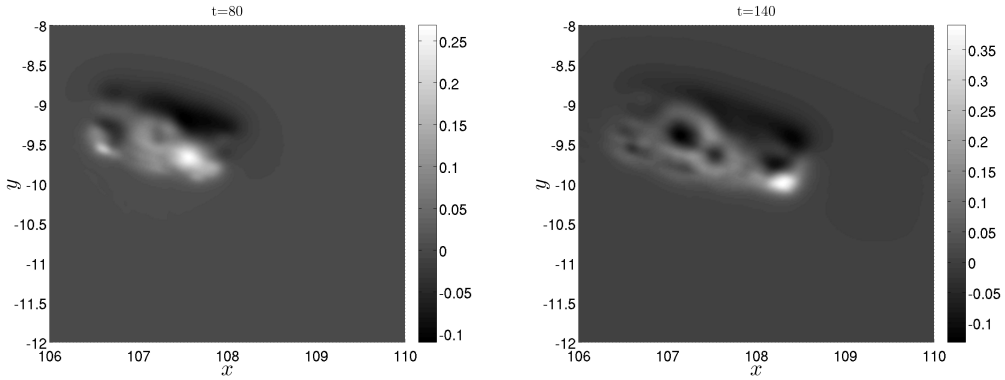

(c) $t = 80\ s$

(d) $t = 140\ s$

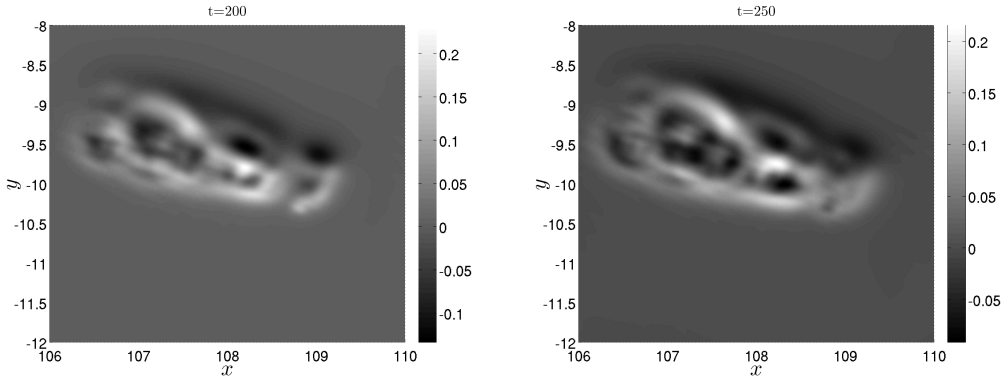

(e) $t = 200\ s$

(f) $t = 250\ s$

FIGURE 8. Snapshots of the free surface elevation computed with the Weakly Nonlinear (WN) model. Water waves are generated by dynamic co-seismic bottom displacements (2.1) reconstructed using the corresponding finite fault solution [Ji06].

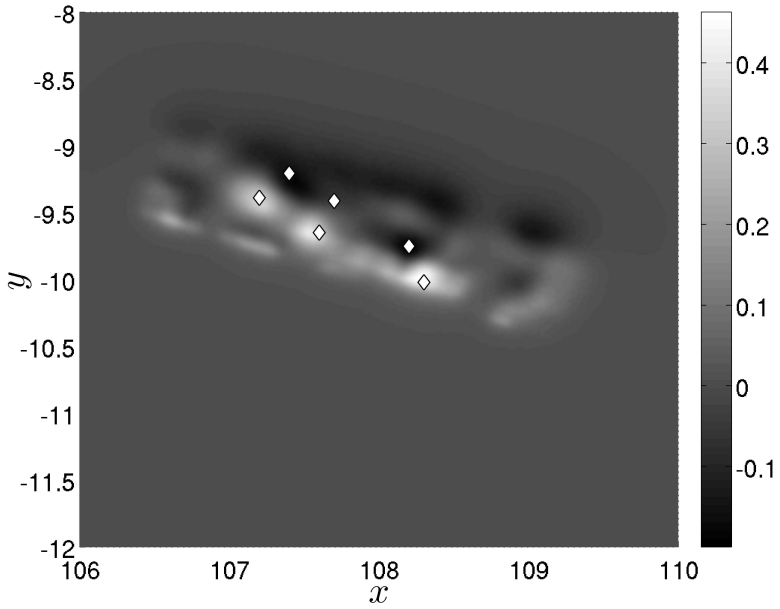

FIGURE 9. Location of the six numerical wave gauges (indicated by the symbol $\diamond$) superposed with the static co-seismic bottom displacement.

along with the static sea bed displacement. Wave gauges are intentionally put in places where the largest waves were expected.

The six wave gauge records are presented in Figures 10 (a) – (f). The first impression is that the overall agreement among all models is satisfactory. We underline that the CP solution is very close to other solutions despite the fact that bathymetric features are neglected. We also note that the specific BBM-BBM type system underestimates by a small amount the maximum wave amplitude compared to the WN model. Our further numerical tests showed some sensitivity of the BBM-BBM solution to the bottom motion scenario [DD07d]. Namely, we can report, for example, that the exponential scenario led to a slight overestimation of the wave amplitude comparing to other models.

5. Conclusions and perspectives

In the present work we considered an important problem of the tsunami generation modeling. Namely, a new method for dynamic co-seismic sea bed displacements construction was proposed. This method basically relies on two main ingredients:

- the finite fault solution [BLM00, JWH02] giving us the slip distribution along the fault
- dynamic sea bed deformation scenarios [Ham73, DDK06, DD07d] allowing us to take into account available information of the rupture dynamics

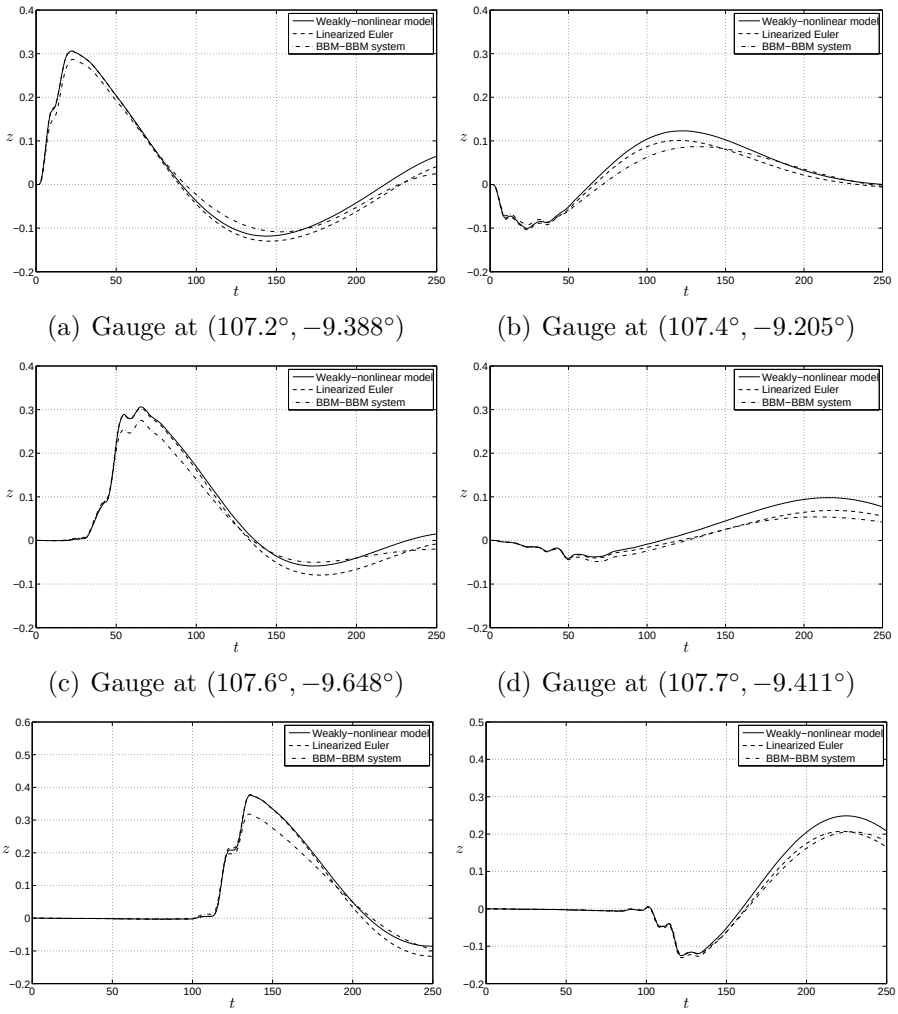

(a) Gauge at $(107.2°, -9.388°)$ (b) Gauge at $(107.4°, -9.205°)$

(c) Gauge at $(107.6°, -9.648°)$ (d) Gauge at $(107.7°, -9.411°)$

(e) Gauge at $(108.3°, -10.02°)$ (f) Gauge at $(108.2°, -9.75°)$

FIGURE 10. Free surface elevation computed numerically at six wave gauges located approximately at the local extrema of the static bottom displacement. The vertical axis is represented in meters.

To our knowledge, this reconstruction of the bottom motion is new. All developments presented in this paper are illustrated on the example of the July, 17 2006 Java event.

Along with the bottom motion construction, we discussed three models to solve approximately the corresponding hydrodynamic problem and compute the induced free surface motions. The July 17, 2006 tsunami generation case was computed with three different models and a comparison was performed. We obtained a surprisingly good agreement between the CP solution and the solutions of the other two models. Recall that in the latter the bottom is assumed to be flat. Some discrepancies might appear later in time since the bathymetry plays a crucial role in the tsunami propagation.

Taking into account the simplicity and the relatively good accuracy of the new WN approximation to the full water wave problem with time dependent variable bottom, we suggest its use for the computation of the initial stages ($\approx 300\ s$) of tsunami's life. The propagation and runup can be computed afterwards by other sophisticated tools [TG97, IYO06, SBT+07, DPD10] some of them being already integrated into tsunami warning systems [TGB+05, WL08].

However we point out that extreme runup values measured after the July, 17 Java 2006 event [FKM+07] are still to be investigated in future studies.

6. Appendix I: Finite fault parameters

Table 3: Subfault parameters given by the finite fault inversion [Ji06].

Lattitude, °	Longitude, °	Depth, km	Slip, cm	Rake, °
-10.33298	109.17112	6.81260	5.01844	121.65860
-10.28919	109.04183	6.81260	4.31652	80.93857
-10.24541	108.91254	6.81260	48.94745	85.43047
-10.20162	108.78325	6.81260	3.60585	101.68500
-10.15784	108.65396	6.81260	0.86479	67.04596
-10.11405	108.52467	6.81260	0.96921	99.45411
-10.07027	108.39538	6.81260	0.62447	71.54340
-10.02648	108.26609	6.81260	0.02449	99.44887
-9.98270	108.13680	6.81260	2.71502	119.63240
-9.93891	108.00751	6.81260	0.57000	114.25760
-9.89513	107.87822	6.81260	14.54725	112.71920
-9.85134	107.74893	6.81260	31.66312	107.26750
-9.80756	107.61964	6.81260	2.74176	85.79224
-9.76377	107.49035	6.81260	3.35868	78.97166
-9.71999	107.36105	6.81260	67.95367	64.89334
-9.67620	107.23177	6.81260	62.33453	65.43832
-9.63242	107.10248	6.81260	35.33318	66.90181
-9.58863	106.97318	6.81260	1.75233	101.93900
-9.54485	106.84389	6.81260	40.63542	81.77631
-9.50106	106.71461	6.81260	84.20831	68.95723
-9.45728	106.58531	6.81260	25.12981	66.62241
-10.24093	109.20313	8.78887	0.68254	88.79068
-10.19714	109.07384	8.78887	30.70282	97.90491
-10.15336	108.94455	8.78887	76.07102	99.93182
-10.10957	108.81525	8.78887	0.56201	79.59160
-10.06579	108.68597	8.78887	0.95023	114.32920
-10.02201	108.55668	8.78887	64.78191	121.81120
-9.97822	108.42738	8.78887	81.31910	105.21240
-9.93443	108.29810	8.78887	137.60680	121.72020

Continued on the next page

Lattitude, °	Longitude, °	Depth, *km*	Slip, *cm*	Rake, °
-9.89065	108.16881	8.78887	85.81732	88.13734
-9.84686	108.03951	8.78887	30.61069	80.38488
-9.80308	107.91022	8.78887	60.08308	113.75000
-9.75929	107.78094	8.78887	46.98381	96.25403
-9.71551	107.65164	8.78887	21.69421	80.82516
-9.67173	107.52235	8.78887	11.01957	112.63110
-9.62794	107.39307	8.78887	27.85978	75.88463
-9.58416	107.26377	8.78887	5.96505	77.66200
-9.54037	107.13448	8.78887	3.85634	83.57522
-9.49658	107.00520	8.78887	3.23158	113.73070
-9.45280	106.87590	8.78887	29.89915	116.10890
-9.40902	106.74661	8.78887	65.25044	72.60931
-9.36523	106.61732	8.78887	19.62932	65.99193
-10.14888	109.23514	10.76514	20.60663	124.43320
-10.10510	109.10584	10.76514	69.91051	122.64720
-10.06131	108.97655	10.76514	63.10052	99.23547
-10.01753	108.84727	10.76514	0.63700	74.09311
-9.97374	108.71797	10.76514	1.02761	117.53560
-9.92996	108.58868	10.76514	85.54328	123.64950
-9.88617	108.45940	10.76514	167.18620	104.56840
-9.84239	108.33010	10.76514	202.60880	122.12460
-9.79860	108.20081	10.76514	144.76970	81.50333
-9.75482	108.07152	10.76514	53.97212	72.84430
-9.71103	107.94223	10.76514	79.21021	98.66053
-9.66725	107.81294	10.76514	82.95619	80.81979
-9.62346	107.68365	10.76514	119.13390	74.36982
-9.57968	107.55436	10.76514	95.90159	116.24710
-9.53589	107.42507	10.76514	36.94965	102.32060
-9.49211	107.29578	10.76514	0.28681	81.49704
-9.44832	107.16649	10.76514	8.06018	98.40840
-9.40454	107.03720	10.76514	3.02927	116.89820
-9.36075	106.90791	10.76514	10.73559	74.60908
-9.31697	106.77862	10.76514	57.94233	75.39254
-9.27318	106.64933	10.76514	60.97223	64.77096
-10.05684	109.26714	12.74141	21.97392	121.10740
-10.01305	109.13785	12.74141	74.47045	119.75060
-9.96927	109.00856	12.74141	17.25334	124.09410
-9.92548	108.87927	12.74141	14.38904	87.41515
-9.88170	108.74998	12.74141	3.03040	106.36440
-9.83791	108.62069	12.74141	8.97587	101.53580
-9.79413	108.49140	12.74141	114.85160	115.94270
-9.75034	108.36211	12.74141	91.90382	115.95240
-9.70656	108.23282	12.74141	64.72478	100.08050
-9.66277	108.10353	12.74141	17.30368	123.06770

Continued on the next page

Lattitude, °	Longitude, °	Depth, km	Slip, cm	Rake, °
-9.61899	107.97424	12.74141	57.09099	68.20686
-9.57520	107.84495	12.74141	64.81193	79.84035
-9.53142	107.71566	12.74141	131.04410	76.45924
-9.48763	107.58636	12.74141	112.11020	99.51801
-9.44385	107.45708	12.74141	60.23628	97.77266
-9.40006	107.32778	12.74141	126.96870	80.27277
-9.35628	107.19849	12.74141	63.39000	65.00801
-9.31249	107.06921	12.74141	0.52621	94.79313
-9.26871	106.93991	12.74141	1.52171	66.78681
-9.22492	106.81062	12.74141	10.96743	81.94861
-9.18114	106.68134	12.74141	2.38062	123.04830
-9.96479	109.29915	14.71768	22.40949	123.90350
-9.92100	109.16986	14.71768	48.62879	115.45630
-9.87722	109.04057	14.71768	5.99559	83.81007
-9.83343	108.91128	14.71768	7.22945	123.80940
-9.78965	108.78199	14.71768	0.10031	93.40998
-9.74586	108.65269	14.71768	0.36991	69.37087
-9.70208	108.52341	14.71768	104.18760	123.83230
-9.65829	108.39411	14.71768	46.12533	95.97049
-9.61451	108.26482	14.71768	0.28679	89.56866
-9.57072	108.13554	14.71768	2.06597	80.14312
-9.52694	108.00624	14.71768	30.55070	66.23147
-9.48315	107.87695	14.71768	73.72994	87.91253
-9.43937	107.74767	14.71768	112.90700	92.28181
-9.39558	107.61837	14.71768	74.73608	86.51558
-9.35180	107.48908	14.71768	121.73820	64.68654
-9.30801	107.35979	14.71768	231.20940	65.50779
-9.26423	107.23050	14.71768	96.55727	87.01543
-9.22044	107.10121	14.71768	28.29534	122.55670
-9.17666	106.97192	14.71768	0.84110	70.21989
-9.13287	106.84263	14.71768	7.99213	87.51706
-9.08909	106.71334	14.71768	1.33281	96.33266
-9.87274	109.33115	16.69394	43.31154	121.79150
-9.82896	109.20187	16.69394	87.17052	124.49750
-9.78517	109.07257	16.69394	61.47630	87.10537
-9.74139	108.94328	16.69394	31.53286	70.58137
-9.69760	108.81400	16.69394	0.70628	65.17896
-9.65382	108.68470	16.69394	5.74160	87.70702
-9.61003	108.55541	16.69394	93.47714	107.32000
-9.56625	108.42612	16.69394	93.55753	85.39201
-9.52246	108.29683	16.69394	47.25525	74.24297
-9.47868	108.16754	16.69394	24.65230	124.20110
-9.43489	108.03825	16.69394	35.63115	71.78733
-9.39111	107.90896	16.69394	25.11757	75.27779

Continued on the next page

Lattitude, °	Longitude, °	Depth, *km*	Slip, *cm*	Rake, °
-9.34732	107.77967	16.69394	68.15302	107.42980
-9.30354	107.65038	16.69394	24.66007	112.77880
-9.25975	107.52109	16.69394	0.50688	79.86887
-9.21597	107.39180	16.69394	119.92850	75.03103
-9.17218	107.26250	16.69394	77.08335	110.83160
-9.12840	107.13322	16.69394	31.65430	123.83060
-9.08461	107.00393	16.69394	11.42768	66.47282
-9.04083	106.87463	16.69394	33.80650	115.65650
-8.99704	106.74535	16.69394	39.47481	65.15574
-9.78069	109.36316	18.67021	35.42621	111.95830
-9.73691	109.23387	18.67021	103.05030	124.62650
-9.69312	109.10458	18.67021	101.38220	122.70620
-9.64934	108.97529	18.67021	76.76701	68.20042
-9.60556	108.84600	18.67021	10.71945	77.79713
-9.56177	108.71671	18.67021	1.32449	100.72950
-9.51799	108.58742	18.67021	37.46857	124.59330
-9.47420	108.45813	18.67021	118.99580	100.38000
-9.43042	108.32883	18.67021	79.62616	91.56905
-9.38663	108.19955	18.67021	97.61735	109.86430
-9.34285	108.07026	18.67021	87.67753	87.57239
-9.29906	107.94096	18.67021	15.14859	64.75201
-9.25528	107.81168	18.67021	82.60960	71.66805
-9.21149	107.68239	18.67021	66.06397	98.55843
-9.16771	107.55309	18.67021	0.43085	67.81042
-9.12392	107.42381	18.67021	35.30429	124.04570
-9.08014	107.29452	18.67021	59.17323	124.55130
-9.03635	107.16522	18.67021	15.23214	66.82615
-8.99257	107.03593	18.67021	28.10358	76.08198
-8.94878	106.90664	18.67021	48.09923	124.24450
-8.90500	106.77735	18.67021	42.38682	124.42850

7. Appendix II: Zakharov's formulation of the water wave problem

In the present section we are going to recast governing equations (3.5) – (3.8) of the water wave problem in more compact and mathematically more convenient form [Zak68, CS93].

Using the definition of the normal velocity (3.10), it is straightforward to rewrite the kinematic free surface condition (3.6):

$$\partial_t \eta - \mathcal{D}_\eta(\varphi) = 0.$$

The time derivative and the horizontal gradient of the velocity potential trace at the free surface can be computed:

$$\partial_t \varphi = \partial_t \phi + \partial_t \eta \, \partial_z \phi|_{z=\eta} = \partial_t \phi + \mathcal{D}_\eta(\varphi) \, \partial_z \phi|_{z=\eta} \,, \tag{7.1}$$

and similarly one can compute the horizontal gradient:

$$\nabla\varphi = \nabla\phi|_{z=\eta} + \nabla\eta\, \partial_z\phi|_{z=\eta}\,, \tag{7.2}$$

In order to close the system, we have to express all derivatives of the potential ϕ computed at the free surface, in terms of φ, η and $\mathcal{D}_\eta(\varphi)$.

From the definition of the normal velocity (3.10) and the D2N operator one readily obtains:

$$\nabla\phi|_{z=\eta} \cdot \nabla\eta = \partial_z\phi|_{z=\eta} - \mathcal{D}_\eta(\varphi). \tag{7.3}$$

Substituting the last identity into (7.2) multiplied by $\nabla\eta$, leads to the following expression:

$$\partial_z\phi|_{z=\eta} = \frac{\mathcal{D}_\eta(\varphi) + \nabla\varphi\cdot\nabla\eta}{1+|\nabla\eta|^2}. \tag{7.4}$$

Now we have all elements to find the horizontal derivatives of the velocity potential:

$$\nabla\phi|_{z=\eta} = \nabla\varphi - \nabla\eta\, \partial_z\phi|_{z=\eta} = \frac{(1+|\nabla\eta|^2)\nabla\varphi - \mathcal{D}_\eta(\varphi)\nabla\eta - (\nabla\varphi\cdot\nabla\eta)\nabla\eta}{1+|\nabla\eta|^2}. \tag{7.5}$$

In order to rewrite Bernoulli condition (3.7) in new variables, we make the following observation (using (7.2) and (7.3)):

$$\begin{aligned}
&\tfrac{1}{2}|\nabla\phi|^2 + \tfrac{1}{2}(\partial_z\phi)^2 = \tfrac{1}{2}\nabla\phi\cdot\nabla\phi + \tfrac{1}{2}\partial_z\phi\,\partial_z\phi = \\
&= \tfrac{1}{2}\nabla\phi\cdot(\nabla\varphi - \partial_z\phi\nabla\eta) + \tfrac{1}{2}\partial_z\phi(\mathcal{D}_\eta(\varphi) + \nabla\phi\cdot\nabla\eta) = \tfrac{1}{2}\nabla\phi\cdot\nabla\varphi + \tfrac{1}{2}\mathcal{D}_\eta(\varphi)\partial_z\phi, \quad z=\eta.
\end{aligned}$$

Taking into account this observation and expression (7.1) for the time derivative of φ, the Bernoulli condition takes this equivalent form:

$$\partial_t\varphi + g\eta + \tfrac{1}{2}\nabla\phi\cdot\nabla\varphi - \tfrac{1}{2}\mathcal{D}_\eta(\varphi)\partial_z\phi = 0, \quad z=\eta.$$

After substituting expressions (7.4), (7.5) into the last equation and summarizing all the developments made above, we get the following set of dynamic equations equivalent to the complete water wave problem (3.5) – (3.8):

$$\begin{aligned}
\partial_t\eta - \mathcal{D}_\eta(\varphi) &= 0,\\
\partial_t\varphi + \tfrac{1}{2}|\nabla\varphi|^2 + g\eta - \tfrac{1}{2(1+|\nabla\eta|^2)}\big[\mathcal{D}_\eta(\varphi) + \nabla\varphi\cdot\nabla\eta\big]^2 &= 0.
\end{aligned}$$

8. Appendix III: Relations between elastic constants

In the classical elasticity theory, coefficients in Lamé equations (governing the displacements field in an elastic solid), can be expressed in terms of various sets of physical parameters [Lov44, SS46]. The purpose of this Appendix is to recall some relations between them.

Lamé coefficients λ and μ can be defined in terms of the Young's modulus E (having the dimension of the pressure $[Pa]$) and Poisson's ratio ν (dimensionless coefficient $0 < \nu < 1/2$):

$$\lambda = \frac{E\nu}{(1+\nu)(1-2\nu)}, \quad \mu = \frac{E}{2(1+\nu)},$$

and inversely:

$$E = \frac{(3\lambda + 2\mu)\mu}{\lambda + \mu}, \quad \nu = \frac{\lambda}{2(\lambda + \mu)}.$$

The celerities of P and S waves have the following expressions in terms of Lamé coefficients:

$$c_p = \sqrt{\frac{\lambda + 2\mu}{\rho}}, \quad c_s = \sqrt{\frac{\mu}{\rho}},$$

where ρ is the density of elastic medium. It is straightforward to invert last relations:

$$\mu = \rho c_s^2, \quad \lambda = \rho c_p^2 - 2\mu.$$

Acknowledgement

D. Dutykh acknowledges the support from French Agence Nationale de la Recherche, project MathOcean (Grant ANR-08-BLAN-0301-01) and Ulysses Program of the French Ministry of Foreign Affairs under the project 23725ZA. The work of D. Mitsotakis was supported by Marie Curie Fellowship No. PIEF-GA-2008-219399 of the European Commission.

We would like to thank Professors Didier Clamond and Frédéric Dias for very helpful discussions on numerical simulation of water waves.

Special thanks go to Professor Costas Synolakis whose works on tsunami waves have also been the source of our inspiration.

References

[AKLV06] C. J. Ammon, H. Kanamori, T. Lay, and A. A. Velasco. The 17 July 2006 Java tsunami earthquake. *Geophysical Research Letters*, 33:L24308, 2006. 2, 4

[Bas06] R. Basher. Global early warning systems for natural hazards: Systematic and people-centred. *Philosophical Transactions: Mathematical, Physical and Engineering Sciences*, 364(1845):2167–2182, 2006. 1

[BLM00] C. Bassin, G. Laske, and G. Masters. The current limits of resolution for surface wave tomography in North America. *EOS Trans AGU*, 81:F897, 2000. 2, 4, 20

[Bou72] J. Boussinesq. Théorie des ondes et des remous qui se propagent le long d'un canal rectangulaire horizontal, en communiquant au liquide contenu dans ce canal des vitesses sensiblement pareilles de la surface au fond. *J. Math. Pures Appl.*, 17:55–108, 1872. 14

[Cau27] A.-L. Cauchy. Mémoire sur la théorie de la propagation des ondes à la surface d'un fluide pesant d'une profondeur indéfinie. *Mém. Présentés Divers Savans Acad. R. Sci. Inst. France*, 1:3–312, 1827. 9

[CM85] R.R. Coifman and Y. Meyer. Nonlinear harmonic analysis and analytic dependence. *Proc, symp. Pure Math*, 43:71–78, 1985. 11

[CS93] W. Craig and C. Sulem. Numerical simulation of gravity waves. *J. Comput. Phys.*, 108:73–83, 1993. 11, 25

[CSS92] W. Craig, C. Sulem, and P.-L. Sulem. Nonlinear modulation of gravity waves: a rigorous approach. *Nonlinearity*, 5(2):497–522, 1992. 11

[CT65] J.W. Cooley and J.W. Tukey. An algorithm for the machine calculation of complex Fourier series. *Math. Comput*, 19:297–301, 1965. 11

[DB06] F. Dias and T.J. Bridges. The numerical computation of freely propagating time-dependent irrotational water waves. *Fluid Dynamics Research*, 38:803–830, 2006. 11

[DD07a] F. Dias and D. Dutykh. *Extreme Man-Made and Natural Hazards in Dynamics of Structures*, chapter Dynamics of tsunami waves, pages 35–60. Springer, 2007. 4, 10

[DD07b] D. Dutykh and F. Dias. Dissipative Boussinesq equations. *C. R. Mecanique*, 335:559–583, 2007. 14

[DD07c] D. Dutykh and F. Dias. Viscous potential free-surface flows in a fluid layer of finite depth. *C. R. Acad. Sci. Paris, Ser. I*, 345:113–118, 2007. 10

[DD07d] D. Dutykh and F. Dias. Water waves generated by a moving bottom. In Anjan Kundu, editor, *Tsunami and Nonlinear waves*. Springer Verlag (Geo Sc.), 2007. 1, 2, 3, 4, 5, 7, 9, 10, 20

[DD09] D. Dutykh and F. Dias. Tsunami generation by dynamic displacement of sea bed due to dip-slip faulting. *Mathematics and Computers in Simulation*, 80(4):837–848, 2009. 1, 2

[DD10] D. Dutykh and F. Dias. Influence of sedimentary layering on tsunami generation. *Computer Methods in Applied Mechanics and Engineering*, In Press, 2010. 1

[DDK06] D. Dutykh, F. Dias, and Y. Kervella. Linear theory of wave generation by a moving bottom. *C. R. Acad. Sci. Paris, Ser. I*, 343:499–504, 2006. 2, 7, 8, 10, 20

[DDZ08] F. Dias, A.I. Dyachenko, and V.E. Zakharov. Theory of weakly damped free-surface flows: a new formulation based on potential flow solutions. *Physics Letters A*, 372:1297–1302, 2008. 10

[DKK07] A. I. Delis, M. Kazolea, and N. A. Kampanis. A robust high-resolution finite volume scheme for the simulation of long waves over complex domains. *Int. J. Numer. Meth. Fluids*, 56:419–452, 2007. 14

[DMS07] V. A. Dougalis, D. E. Mitsotakis, and J.-C. Saut. On some boussinesq systems in two space dimensions: Theory and numerical analysis. *Math. Model. Num. Anal.*, 41(5):825–254, 2007. 14, 15

[DMS09] V. A. Dougalis, D. E. Mitsotakis, and J.-C. Saut. On initial-boundary value problems for a boussinesq system of bbm-bbm type in a plane domain. *Discrete Contin. Dyn. Syst.*, 23(4):1191–1204, 2009. 14

[DP80] J. R. Dormand and P.J. Prince. A family of embedded Runge-Kutta formulae. *J. Comp. Appl. Math.*, 6:19–26, 1980. 14, 17

[DPD10] D. Dutykh, R. Poncet, and F. Dias. Complete numerical modelling of tsunami waves: generation, propagation and inundation. *Submitted*, 2010. 1, 2, 14, 22

[dSV71] A.J.C. de Saint-Venant. Théorie du mouvement non-permanent des eaux, avec application aux crues des rivières et à l'introduction des marées dans leur lit. *C. R. Acad. Sc. Paris*, 73:147–154, 1871. 14

[Dut07] D. Dutykh. *Mathematical modelling of tsunami waves*. PhD thesis, École Normale Supérieure de Cachan, 2007. 1, 2, 4, 10

[Dut09a] D. Dutykh. Group and phase velocities in the free-surface visco-potential flow: new kind of boundary layer induced instability. *Physics Letters A*, 373:3212–3216, 2009. 10

[Dut09b] D. Dutykh. Visco-potential free-surface flows and long wave modelling. *Eur. J. Mech. B/Fluids*, 28:430–443, 2009. 10

[FCKG05] D. Fructus, D. Clamond, O. Kristiansen, and J. Grue. An efficient model for threedimensional surface wave simulations. Part i: Free space problems. *J. Comput. Phys.*, 205:665–685, 2005. 11, 13

[FJ05] Matteo Frigo and Steven G. Johnson. The design and implementation of FFTW3. *Proceedings of the IEEE*, 93(2):216–231, 2005. special issue on "Program Generation, Optimization, and Platform Adaptation". 11

[FKM+07] H. M. Fritz, W. Kongko, A. Moore, B. McAdoo, J. Goff, C. Harbitz, B. Uslu, N. Kalligeris, D. Suteja, K. Kalsum, V. V. Titov, A. Gusman, H. Latief, E. Santoso, S. Sujoko, D. Djulkarnaen, H. Sunendar, and C. Synolakis. Extreme runup from the 17 July 2006 Java tsunami. *Geophys. Res. Lett.*, 34:L12602, 2007. 4, 22

[GBM+05] F.I. González, E.N. Bernard, C. Meinig, M.C. Eble, H.O. Mofjeld, and S. Stalin. The NTHMP tsunameter network. *Natural Hazards*, 35:25–39, 2005. 1

[GN07] P. Guyenne and D.P. Nicholls. A high-order spectral method for nonlinear water waves over moving bottom topography. *SIAM J. Sci. Comput.*, 30(1):81–101, 2007. 13

[Ham72] J.L. Hammack. *Tsunamis – A Model of Their Generation and Propagation*. PhD thesis, California Institute of Technology, 1972. 7, 9

[Ham73] J. Hammack. A note on tsunamis: their generation and propagation in an ocean of uniform depth. *J. Fluid Mech.*, 60:769–799, 1973. W. M. Keck Laboratory of Hydraulics and Water Resources, California Institute of Technology, Pasadena. 1, 7, 9, 20

[HNW09] E. Hairer, S.P. Nørsett, and G. Wanner. *Solving ordinary differential equations: Nonstiff problems*. Springer, 2009. 14, 15, 17

[IAK+07] M. Ioualalen, J. Asavanant, N. Kaewbanjak, S.T. Grilli, J.T. Kirby, and P. Watts. Modeling the 26 december 2004 Indian Ocean tsunami: Case study of impact in Thailand. *Journal of Geophysical Research*, 112:C07024, 2007. 2

[Ima96] F. Imamura. *Long-wave runup models*, chapter Simulation of wave-packet propagation along sloping beach by TUNAMI-code, pages 231–241. World Scientific, 1996. 1, 14

[IYO06] F. Imamura, A.C. Yalciner, and G. Ozyurt. *Tsunami modelling manual*, April 2006. 22

[Ji06] C. Ji. Preliminary result of the 2006 July 17 magnitude 7.7 - south of Java, Indonesia earthquake. Technical report, http://neic.usgs.gov/neis/eq_depot/2006/eq_060717_qgaf/neic_qgaf_ff.html, 2006. 4, 5, 6, 7, 19, 22

[JWH02] C. Ji, D. J. Wald, and D. V. Helmberger. Source description of the 1999 Hector Mine, California earthquake; Part I: Wavelet domain inversion theory and resolution analysis. *Bull. Seism. Soc. Am.*, 92(4):1192–1207, 2002. 2, 4, 20

[Kaj63] K. Kajiura. The leading wave of tsunami. *Bull. Earthquake Res. Inst., Tokyo Univ.*, 41:535–571, 1963. 1, 8

[KDD07] Y. Kervella, D. Dutykh, and F. Dias. Comparison between three-dimensional linear and nonlinear tsunami generation models. *Theor. Comput. Fluid Dyn.*, 21:245–269, 2007. 7, 8, 9

[Lam32] H. Lamb. *Hydrodynamics*. Cambridge University Press, 1932. 9

[Lov44] A. E. H. Love. *A treatise on the mathematical theory of elasticity*. Dover Publications, New York, 1944. 26

[MBS03] P. A. Madsen, H. B. Bingham, and H. A. Schaffer. Boussinesq-type formulations for fully nonlinear and extremely dispersive water waves: derivation and analysis. *Proc. R. Soc. Lond. A*, 459:1075–1104, 2003. 14

[Mei94] C.C. Mei. *The applied dynamics of ocean surface waves*. World Scientific, 1994. 9

[Min36] R. D. Mindlin. Force at a point in the interior of a semi-infinite medium. *Physics*, 7:195–202, 1936. 4

[Mit09] D.E. Mitsotakis. Boussinesq systems in two space dimensions over a variable bottom for the generation and propagation of tsunami waves. *Math. Comp. Simul.*, 80:860–873, 2009. 14, 15

[MS67] L. Mansinha and D. E. Smylie. Effect of earthquakes on the Chandler wobble and the secular polar shift. *J. Geophys. Res.*, 72:4731–4743, 1967. 2, 4

[MS71] L. Mansinha and D. E. Smylie. The displacement fields of inclined faults. *Bull. Seism. Soc. Am.*, 61:1433–1440, 1971. 2, 4

[OK06] A. Ozgun Konca. Preliminary result 06/07/17 (Mw 7.9) , Southern Java earthquake. Technical report, http://www.tectonics.caltech.edu/slip_history/2006_s_java/s_java.html, 2006. 4

[Oka85] Y. Okada. Surface deformation due to shear and tensile faults in a half-space. *Bull. Seism. Soc. Am.*, 75:1135–1154, 1985. 2, 4

[Oka92] Y. Okada. Internal deformation due to shear and tensile faults in a half-space. *Bull. Seism. Soc. Am.*, 82:1018–1040, 1992. 2, 4

[OTM01] T. Ohmachi, H. Tsukiyama, and H. Matsumoto. Simulation of tsunami induced by dynamic displacement of seabed due to seismic faulting. *Bull. Seism. Soc. Am.*, 91:1898–1909, 2001. 2

[Per67] D. H. Peregrine. Long waves on a beach. *J. Fluid Mech.*, 27:815–827, 1967. 15

[Pre65] F. Press. Displacements, strains and tilts at tele-seismic distances. *J. Geophys. Res.*, 70:2395–2412, 1965. 4

[RLF+08] A. B. Rabinovich, L. I. Lobkovsky, I. V. Fine, R.E. Thomson, T. N. Ivelskaya, and E. A. Kulikov. Near-source observations and modeling of the Kuril Islands tsunamis of 15 November 2006 and 13 January 2007. *Adv. Geosci.*, 14:105–116, 2008. 2

[SB06] C.E. Synolakis and E.N. Bernard. Tsunami science before and beyond Boxing Day 2004. *Phil. Trans. R. Soc. A*, 364:2231–2265, 2006. 1, 2

[SBT+07] C.E. Synolakis, E.N. Bernard, V.V. Titov, U. Kanoglu, and F.I. Gonzalez. Standards, criteria, and procedures for NOAA evaluation of tsunami numerical models. Technical report, NOAA/Pacific Marine Environmental Laboratory, 2007. 22

[SF09] T. Saito and T. Furumura. Three-dimensional tsunami generation simulation due to sea-bottom deformation and its interpretation based on the linear theory. *Geophys. J. Int.*, 178:877–888, 2009. 2, 9

[SS46] I. S. Sokolnikoff and R. D. Specht. *Mathematical theory of elasticity.* McGraw-Hill, New York, 1946. 26

[Sto58] J.J. Stoker. *Water waves, the mathematical theory with applications.* Wiley, 1958. 9, 14

[Syn05] C. Synolakis. India must cooperate on tsunami warning system. *Nature*, 434:17–18, 2005. 1

[Tan86] M. Tanaka. The stability of solitary waves. *Phys. Fluids*, 29(3):650–655, 1986. 15, 16

[TDS07] P. Tkalich, M.H. Dao, and C.E. Soon. Tsunami propagation modeling and forecasting for early warning system. *Journal of Earthquake and Tsunami*, 1(1):87–98, 2007. 1

[TG97] V.V. Titov and F.I. González. Implementation and testing of the method of splitting tsunami (MOST) model. Technical Report ERL PMEL-112, Pacific Marine Environmental Laboratory, NOAA, 1997. 1, 14, 22

[TGB+05] V.V. Titov, F.I. Gonzalez, E. N. Bernard, M.C. Eble, H.O. Mofjeld, J.C. Newman, and A.J. Venturato. Real-time tsunami forecasting: Challenges and solutions. *Natural Hazards*, 35:41–58, 2005. 1, 22

[THT02] M.I. Todorovska, A. Hayir, and M.D. Trifunac. A note on tsunami amplitudes above submarine slides and slumps. *Soil Dynamics and Earthquake Engineering*, 22:129–141, 2002. 7

[TS98] V. V. Titov and C. E. Synolakis. Numerical modeling of tidal wave runup. *J. Waterway, Port, Coastal, and Ocean Engineering*, 124:157–171, 1998. 14

[TT01] M. I. Todorovska and M. D. Trifunac. Generation of tsunamis by a slowly spreading uplift of the seafloor. *Soil Dynamics and Earthquake Engineering*, 21:151–167, 2001. 1, 7, 9

[Vol07] V. Volterra. Sur l'équilibre des corps élastiques multiplement connexes. *Annales Scientifiques de l'Ecole Normale Supérieure*, 24(3):401–517, 1907. 4

[Whi99] G.B. Whitham. *Linear and nonlinear waves.* John Wiley & Sons Inc., New York, 1999. 10, 14

[WL08] S.A. Weinstein and P.R. Lundgren. Finite fault modeling in a tsunami warning center context. *Pure Appl. Geophys.*, 165:451–474, 2008. 2, 22

[XG09] L. Xu and P. Guyenne. Numerical simulation of three-dimensional nonlinear water waves. *J. Comput. Phys.*, 228(22):8446–8466, 2009. 13

[Yal08] A.C. Yalciner. July 17, 2006 Indonesia Java tsunami. Technical report, http://yalciner.ce.metu.edu.tr/java/, 2008. 3

[Zak68] V.E. Zakharov. Stability of periodic waves of finite amplitude on the surface of a deep fluid. *J. Appl. Mech. Tech. Phys.*, 9:1990–1994, 1968. 10, 11, 25

LAMA, UMR 5127 CNRS, Université de Savoie, Campus Scientifique, 73376 Le Bourget-du-Lac Cedex, France

E-mail address: Denys.Dutykh@univ-savoie.fr

URL: http://www.lama.univ-savoie.fr/~dutykh/

UMR de Mathématiques, Université de Paris-Sud, Bâtiment 425, P.O. Box, 91405 Orsay, France

E-mail address: Dimitrios.Mitsotakis@math.u-psud.fr

URL: http://sites.google.com/site/dmitsot/

LAMA, UMR 5127 CNRS, Université de Savoie, Campus Scientifique, 73376 Le Bourget-du-Lac Cedex, France

E-mail address: Xavier.Gardeil@etu.univ-savoie.fr